Appendix A

List of CD Content

A 1: Simulation videos

A 2: Matlab programs

A 3: PDF prints of web pages, web sources, articles and datasheets.

A 4: The report as PDF file

Appendix B

Dimensionless Numbers

A list of the different dimensionless numbers used in the report.

Name	Equation	Represents
Dean	$D = Re\left(\frac{d}{2R}\right)^{1/2}$	The ratio of the viscous force acting on a fluid flowing in a curved pipe to the centrifugal force.
Eötvös	$Eo = \frac{\Delta\rho g L^2}{\sigma}$	Capillary flows and sloshing that relates the gravity force and the surface tension.
Froude	$Fr = \frac{U^2}{gD}$	A measure of the inertial force and the gravitational force.
Kutateladze	$Ku = \frac{U\rho^{1/2}}{(g\Delta\rho\sigma)^{1/4}}$	A balance between the dynamic head, surface tension and gravitational force.
Reynolds	$Re = \frac{\rho UD}{\mu}$	The ratio of inertial forces to the viscous forces.

Table B.1: The dimensionless numbers in alphabetical order [Awad, 2012]

Appendix C

Two-Phase Fluid Properties

This appendix outlines the basic equations regarding two-phase flow, which are used in the report.

The two-phase fluid can only be defined as completely homogeneously mixed, if the gas and liquid fractions are equal whether they are defined by the volume, area or line average. [Time, 2009]

The two-phase fluid behaviour can be described by a set of equations, which are based on Figure C.1. The parameters are area A, the volume flow $\dot{Q}$ and velocity U. The subscripts l and g represent the liquid and gas part.

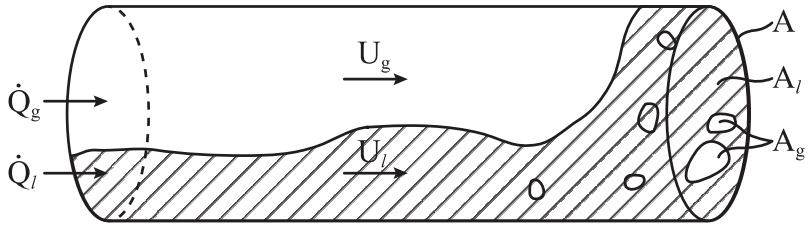

Figure C.1: Two-phase fluid parameters in a pipe

If the two-phase fluid is homogeneously mixed the no-slip fractions are defined based on the volume flow, $\dot{Q}$, see Equation (C.1).

$$\lambda_l = \frac{\dot{Q}_l}{\dot{Q}_l + \dot{Q}_g} \qquad \lambda_g = \frac{\dot{Q}_g}{\dot{Q}_l + \dot{Q}_g} \tag{C.1}$$

Slip is present if the fluid is not completely homogeneously. The slip equation (C.2) is equal to one, when the fluid is a completely homogeneously mixture, where the phase velocities for the two phases are equal.

$$S = \frac{U_g}{U_l} \tag{C.2}$$

Here the phase velocities for the two phases are defined:

$$U_l = \frac{\dot{Q}_l}{A_l} \qquad U_g = \frac{\dot{Q}_g}{A_g} \tag{C.3}$$

When slip is present the no-slip fractions are not equal to the fluid fractions. The fluid fractions can be seen in Equation (C.4) and (C.5) calculated with the slip, the volume flow rate and the superficial velocities.

$$\epsilon_l = \frac{\dot{Q}_l}{\dot{Q}_l + \frac{1}{S}\dot{Q}_g} = \frac{U_{ls}}{U_{ls} + \frac{1}{S}U_{gs}} \tag{C.4}$$

$$\epsilon_g = \frac{\dot{Q}_g}{S \cdot \dot{Q}_l + \dot{Q}_g} = \frac{U_{gs}}{S \cdot U_{ls} + U_{gs}} \tag{C.5}$$

The superficial velocities for the gas and liquid phases can be seen in Equation (C.6). The mixture velocity is the two superficial velocities added together.

$$U_{ls} = \frac{\dot{Q}_l}{A} \qquad U_{gs} = \frac{\dot{Q}_g}{A} \tag{C.6}$$

The mixture mass flow is approximately equal to the liquid mass flow, due to much smaller density of the gas compared to the liquid, as seen in Equation (C.7).

$$\begin{aligned} \dot{m}_{\text{mix}} &= \dot{m}_g + \dot{m}_l \approx \dot{m}_l \\ &= \rho_g \dot{Q}_g + \rho_l \dot{Q}_l \approx \rho_l \dot{Q}_l \end{aligned} \tag{C.7}$$

The mixture volume flow is much larger than the volume flow of the liquid due to the gas volume, see Equation (C.8).

$$\dot{Q}_{\text{mix}} = \dot{Q}_g + \dot{Q}_l >> \dot{Q}_l \tag{C.8}$$

The density for a two-phase fluid is defined by the individual densities of the two phases, the gas and fluid fractions [Time, 2009]. The mixture density for a fluid is defined in Equation (C.9).

$$\rho_{\text{mix}} = \epsilon_g \rho_g + \epsilon_l \rho_l \tag{C.9}$$

The viscosity for the mixture is not as well defined as the density, since it depends on the bubble size, flow regimes and other dynamical processes. There are many different models. The Dukler model, Equation (C.10), is based on the same principle as the mixture density in Equation (C.9). The mixture viscosity is defined by the single-phase fluid properties, the gas and fluid fractions.

Dukler:

$$\mu_{\text{mix}} = \epsilon_g \mu_g + (1 - \epsilon_g)\, \mu_l \tag{C.10}$$

The Dukler model will at low gas fractions underestimate the viscosity compared to the Cicchitti viscosity model and overestimate the viscosity at low liquid fractions compared to the McAdams viscosity model [Time, 2009].

The mixture Reynolds number can be defined as in Equation (C.11). The mixture Reynolds number uses the mixture fluid properties.

$$\text{Re}_{\text{mix}} = \frac{\rho_{\text{mix}} U_{\text{mix}} D}{\mu_{\text{mix}}} \tag{C.11}$$

The Coriolis flowmeter measures the mixed fluid mass flow rate and the mixed fluid density. The Gas Void Fraction, GVF is estimated based on standard deviation of the phase shift and density. The GVF is being defined in Equation (C.12). The GVF is the same as the gas fraction in Equation (C.5), when the slip is one (S=1).

$$\begin{aligned} GVF &= \frac{\dot{m}_g \rho_l}{(\dot{m}_l \rho_g + \dot{m}_g \rho_l)} \cdot 100 \\ &= \frac{\dot{Q}_g}{\dot{Q}_l + \dot{Q}_g} \cdot 100 \end{aligned} \tag{C.12}$$

C.1 Speed of Sound

Speed of sound for a dispersed flow regime, as seen in Figure 1.6a in Chapter 1, is described by three equations [Time, 2009]. Equation (C.13) determines the speed of sound for a mixture in a dispersed flow, where c_g and c_l are speed of sound in gas and liquid respectively.

$$c_d = \left[(\epsilon_g \rho_g + \epsilon_l \rho_l) \left(\frac{\epsilon_g}{\rho_g c_g^2} + \frac{\epsilon_l}{\rho_l c_l^2} \right) \right]^{-1/2} \tag{C.13}$$

The speed of sound for liquid can be described with Equation (C.14), where K is the bulk modulus of the liquid; for water K is 2.15 GPa at 15.6°C [Munson et al., 2010].

$$c_l = \sqrt{\frac{K}{\rho_l}} \tag{C.14}$$

The speed of sound for gas is dependent on the pressure due to the compressibility of the gas. Equation (C.15) shows how the speed of sound is found from the pressure and the density. γ is the isentropic expansion factor; 1.4 for adiabatic and 1.0 for isothermal. Equation (C.16) is the ideal gas law.

$$c_g = \sqrt{\gamma \frac{P}{\rho_g}} \tag{C.15}$$

$$\rho_g = \frac{P \cdot M}{R \cdot T} \tag{C.16}$$

Appendix D

Experimental Setup

The experimental setup can be seen in Figure D.1, where the flow is from left to right. The water comes from an open water tank, where the flow is controlled by a pump. A manual ON/OFF valve is connected after the pump. The valve is always open when running tests. After the valve is a Coriolis reference flowmeter connected. The reference flowmeter is a SITRANS FC430. The reference meter measures only the water mass flow and density. After the reference meter there is the air intake. The air intake is controlled with a one way valve and an air supply controller. After the air intake a rubber pipe is connected in order to avoid cross talk between the flowmeters, when testing a Siemens Coriolis flowmeter. Cross talk happens if the flowmeters vibrate with the same frequency and is undesirable. A pressure transducer comes next and then the test meter. After the test meter a second pressure transducer is connected. A automatic valve controlling the back-pressure comes after. Before the water runs back to the tank, the second ON/OFF valve is placed, which is also always open, when running tests.

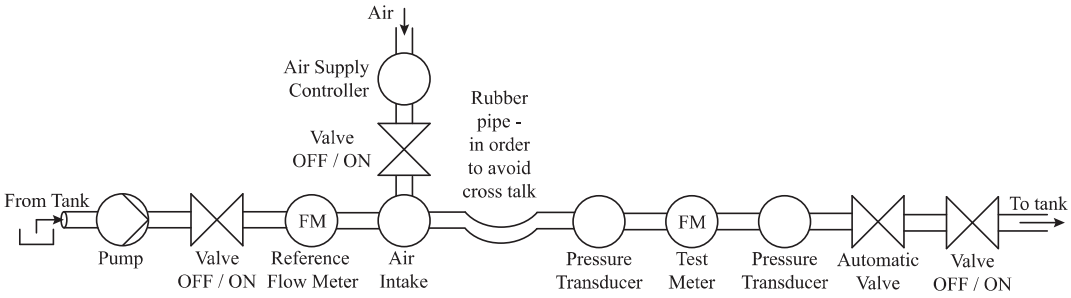

Figure D.1: Sketch of the experimental setup. The flow direction is from left to right. FM indicates a flowmeter

D.1 Experimental Procedures

The water flow rate is set by the pump, the back-pressure by the automatic valve and the air flow rate by the air supply controllers. The set points controlling the GVF, the water flow rate and the back-pressure is set in a batch file, see an example in Table D.1. In Table D.1 it can be seen that the water flow rate and the GVF changes. The program

runs through 60 s where the water flow rate and the back-pressure is set. For the next 60 s air is added to the flow and the measurements are collected. The last 30 s the air flow is zero and the pipe system is emptied for possible air bubbles.

After the first run is finished, the second run starts, where the GVF is increased. When the GVF has increased to 10%, the water flow rate increases to the next set point. The back-pressure is increased when the water flow rate reaches the maximum flow rate setting specified.

Flow rate $\left(\frac{\text{kg}}{\text{h}}\right)$	Back-pressure (mbar)	GVF (%)	Time no air (s)	Time air (s)	Time no air (s)
250	300	0	60	60	30
250	300	0.2	60	60	30
250	300	0.3	60	60	30
250	300	0.5	60	60	30
250	300	0.7	60	60	30
250	300	1	60	60	30
250	300	2	60	60	30
250	300	5	60	60	30
250	300	10	60	60	30
500	300	0	60	60	30
500	300	0.2	60	60	30
500	300	0.3	60	60	30
500	300	0.5	60	60	30
⋮	⋮	⋮	⋮	⋮	⋮

Table D.1: Batch file example. The flow rate is the water flow rate

By having specified the water flow rate, the back-pressure and the GVF, the measurement accuracy of the flowmeter can be found and examined. Chapter 3 contains the results of the measuring.

In order to ensure that the data used in the modelling has the specified GVF, the first 15 s and the last 15 s of the measured data is removed and only 30 s data for each run is collected and used.

D.1.1 Observations during Tests

At low water flow rates and low GVF, air was not supplied to the flow rig. This was due to the air demand was lower, than the minimum level of air the air supply controllers could provide and therefore no air was provided. As the water flow rate increases, the air needed to obtain a certain GVF is over the minimum level the air supply controllers can deliver.

Appendix E

Notes on CFD

Computational Fluid Dynamics, CFD is a computer based simulation tool, which is used to analyse the fluid behaviour in the Coriolis flowmeter. The simulation tool codes are based on numerical algorithms, which can handle the complexity of the fluid flow. Three steps are used when dealing with CFD simulations; pre-processing, solver and post-processing. Figure E.1 shows the general overall structure of a CFD simulation.

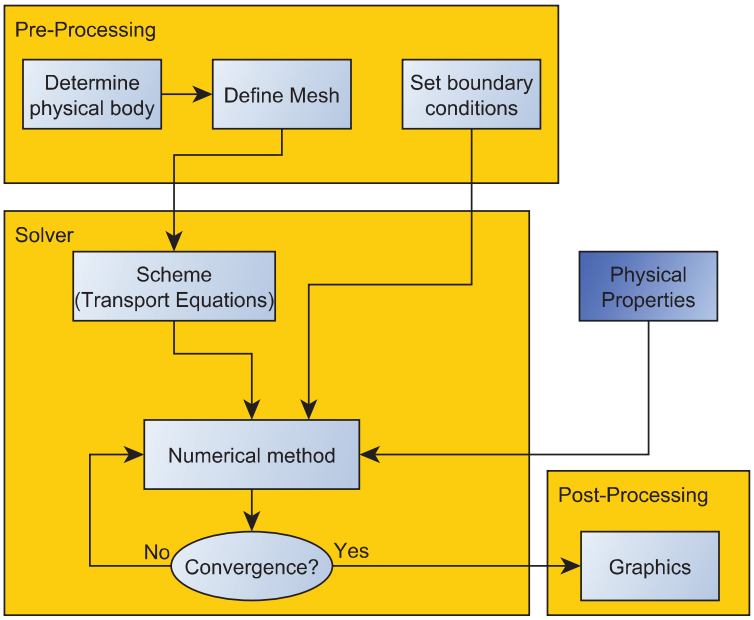

Figure E.1: Overall CFD process [Christensen et al., 2012]

In pre-processing the domain, the mesh and the boundary conditions are defined. In the second step the solver (FLUENT) and the way in which the equations are solved (the scheme) are chosen. In the solver the simulation is set up and runs until the solution has converged. After the solution has converged or the desired time has past, the post-processing begins with evaluation of the simulation results.

E.1 Near-Wall Treatment

Fluid flow is in general impacted by the wall of the flow domain. In order to get a accurate representation of the flow behaviour near the wall, the wall needs to be considered. The near-wall region can be divided into three layers.

1. The **viscous layer** lies closest to the wall. The flow is almost laminar. The viscous layer is also known as the sublayer.
2. The **buffer layer** is the second layer.
3. The **fully turbulent layer** is the outer layer.

There is two ways to solve the near-wall region, these can be seen in Figure E.2. The Wall Function Approach where the two layers closest to the wall are not being solved instead wall functions are used to connect the turbulent layers with the wall. The Wall Function Approach is based on high Reynolds turbulent flow, where the viscous effect near the wall can be neglected. The Near-Wall Model Approach solves the near-wall region with a grid fitted to the two inner layers of the near-wall region.

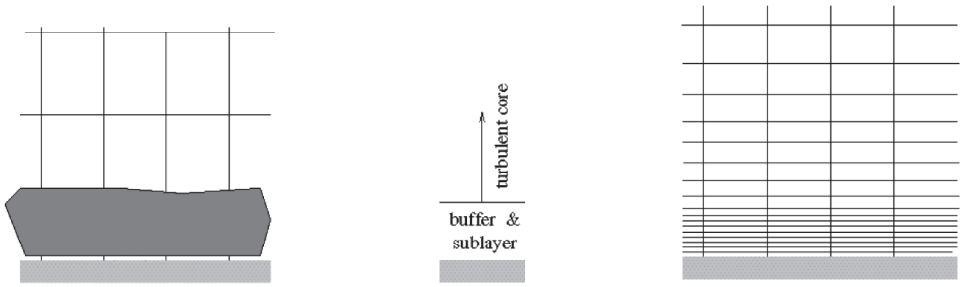

Figure E.2: Near-wall treatment in FLUENT. To the left the Wall Function Approach and to the right the Near-Wall Model Approach [ANSYS, Inc., 2006,p.12-60] (modified)

In Section 4.1 the mesh is designed following the near-wall mesh guidelines in [ANSYS, Inc., 2006,p.12-76] and [ERCOFTAC, 2000] so the viscous and buffer layer are solved accurately.
The near wall mesh guidelines:

- The first row of cells near the wall should have a y^+-value of 1. y^+<4 to 5 is also accepted as long as it is well inside the viscous layer.
- There should be at least 10 cells within the viscous-affected near-wall region

In order to check the design strategy displaying the y^+-value is an effective tool. It should be noted, that the mentioned theories and guidelines are for single-phase fluid simulations.

Appendix F

Grid independence data

The meshes designed and used in the grid independence analysis have all a y^+-value of 5 at the inlet, tube and outlet sections. The cell number of the hybrid unstructured grids vary. The grid independence analysis is performed with a 1 m/s water flow at 20°C with a back-pressure of 300 mbar.

In the following section residual plots and tables with quality indicators as skewness and orthogonal quality for each of the meshes are presented.

The skewness determines how close to ideal a face and/or cell is. Highly skewed cells should be avoided since they produce a less accurate result [ANSYS, Inc., 2012].

Skewness	Cell quality
1	Degenerate
0.9-<1	Bad
0.75-<0.9	Poor
0.5-<0.75	Fair
0.25-<0.5	Good
<0-<0.25	Excellent
0	Equilateral

Table F.1: Skewness indicator [ANSYS, Inc., 2012]

Another indicator of cell quality is the orthogonal quality, where zero orthogonal quality is bad and an orthogonal quality of one is good. The orthogonal quality for a cell is based on the face normal vector, the vector from the cell centroid of each of the adjacent cells and the vector from the cell centroid to each of the faces of the cell. "Orthogonal quality relates to how close the angles between adjacent element faces or adjacent element edges are to some optimal angle (*e.g.* 90° for quadrilateral faced elements and 60° for triangular faces elements.)"[ANSYS, Inc., 2010,Section 14.3.2.1]

In the following sections the residual plot for each of the meshes are presented. The residual plot is used to judge convergence. In FLUENT the default convergence criterion for scaled residuals are 10^{-3}. [ANSYS, Inc., 2006]

The unscaled residual for the continuity equation is defined in Equation (F.1). [ANSYS, Inc., 2006]

$$R^c = \sum_{\text{cells i}} |\text{rate of mass creation in cell i}| \tag{F.1}$$

The scaled residual for the continuity equation can be seen in Equation (F.2).

$$\frac{R^c_{\text{iteration n}}}{R^c_{\text{iteration 5}}} \tag{F.2}$$

The denominator in Equation (F.2) is the largest absolute value of the continuity residual in the first five iterations.

F.1 GCI Mesh

Three meshes are designed and used in a grid convergence study in Section 4.2.1. The following sections show the quality and residual plot for each of the meshes. The residual plots are for the steady single-phase flow simulation.

152356 Cells Mesh

The first mesh has a cell number of 152356 cells.

	Skewness	Orthogonal quality
Minimum	$7.653 \cdot 10^{-3}$	$1.172 \cdot 10^{-3}$
Maximum	0.999	0.993
Average	0.315	0.812
Standard deviation	0.241	0.174

Table F.2: Quality for the 152356 cell mesh

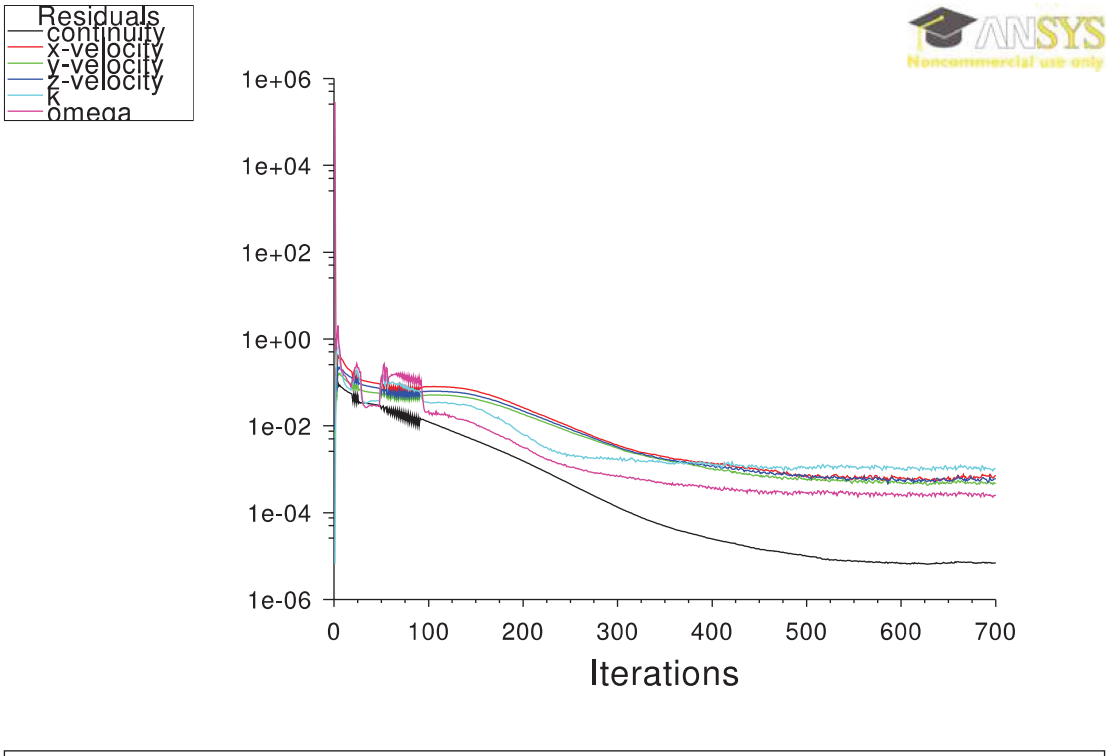

Figure F.1: Residual plot for the 152356 cell mesh

357934 Cells Mesh

The second mesh has a cell number of 357934 cells.

	Skewness	Orthogonal quality
Minimum	$9.988 \cdot 10^{-5}$	$1.417 \cdot 10^{-3}$
Maximum	0.999	0.994
Average	0.271	0.846
Standard deviation	0.171	0.125

Table F.3: Quality for the 357934 cell mesh

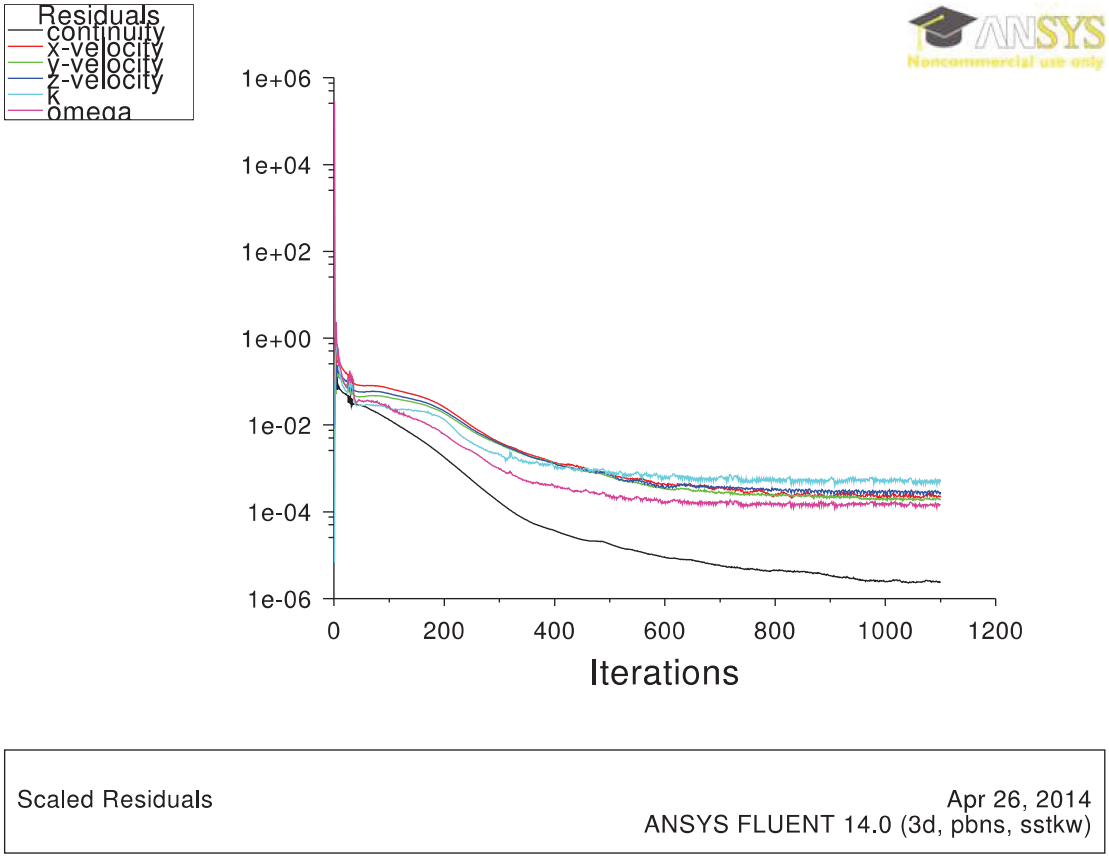

Figure F.2: Residual plot for the 357934 cell mesh

632376 Cells Mesh

The third mesh has a cell number of 632376 cells.

	Skewness	Orthogonal quality
Minimum	$5.901 \cdot 10^{-5}$	$1.466 \cdot 10^{-3}$
Maximum	0.999	0.995
Average	0.246	0.854
Standard deviation	0.145	0.109

Table F.4: Quality for the 632376 cell mesh

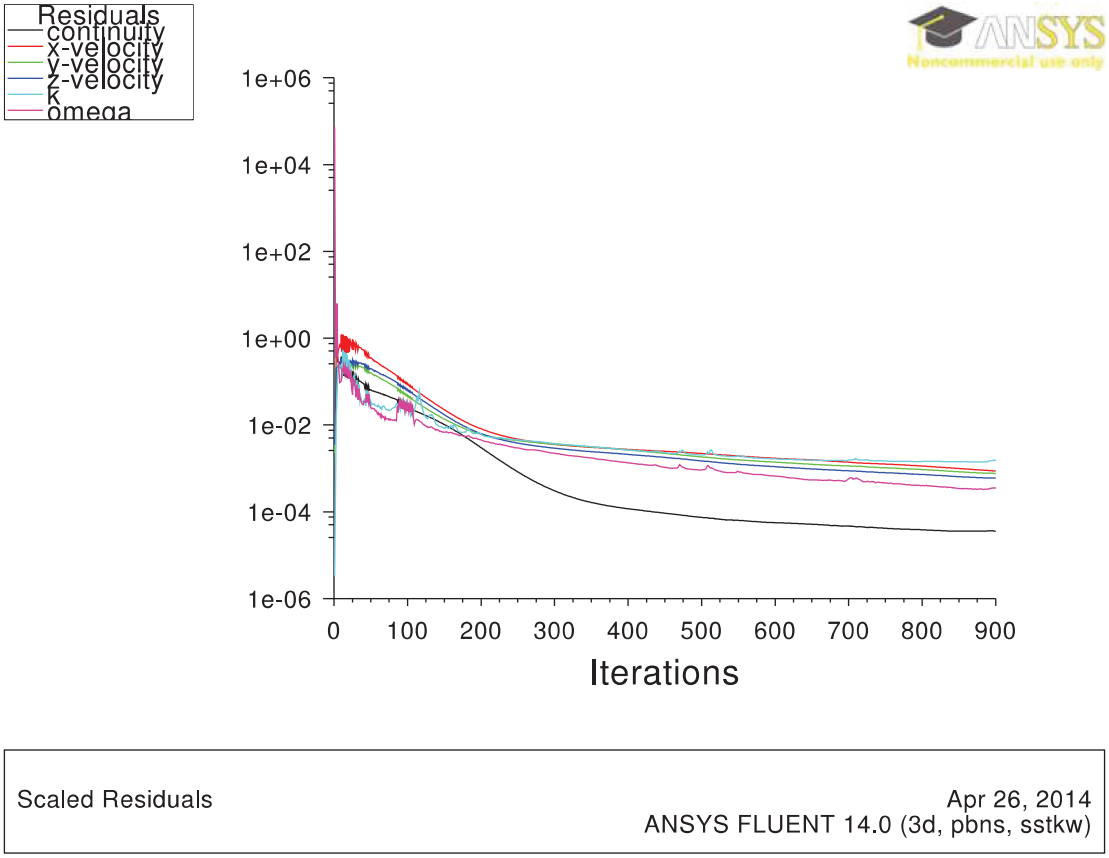

Figure F.3: Residual plot for the 632376 cell mesh

Appendix G

Residual Plots - Cases

The simulations are performed in transient and steady state as seen in Chapter 5. The cases are based on the 152356 cells mesh. Not all the residual plots of the transient simulations are presented here do to the poor resolution of the graphs after several iterations.

Figure G.1 shows the residual plot for the steady single-phase liquid flow case.

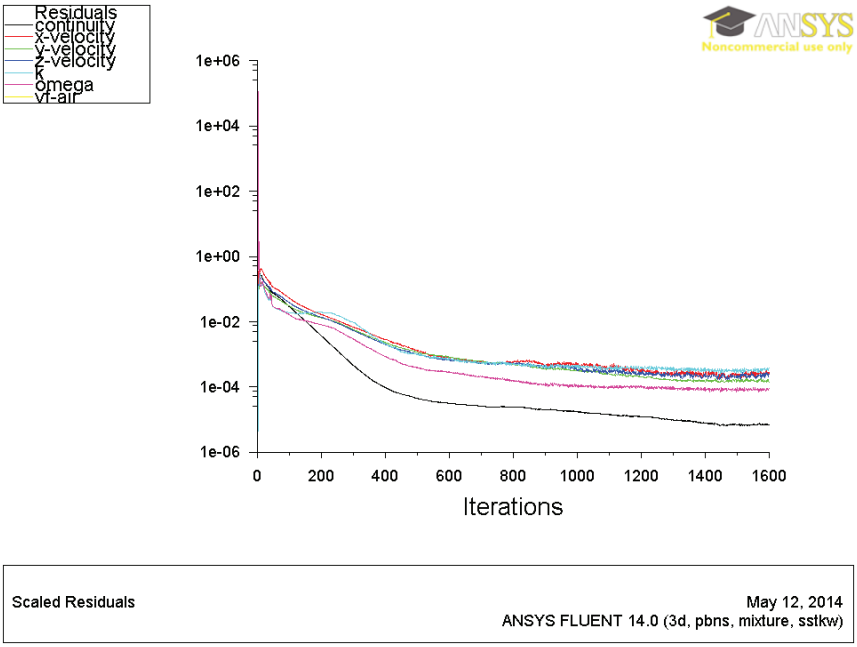

Figure G.1: Residual plot for the steady single-phase liquid flow case

The first part of the residual plot for the transient two-phase case, where the steady single-phase case is the initial guess, can be seen in Figure G.2.

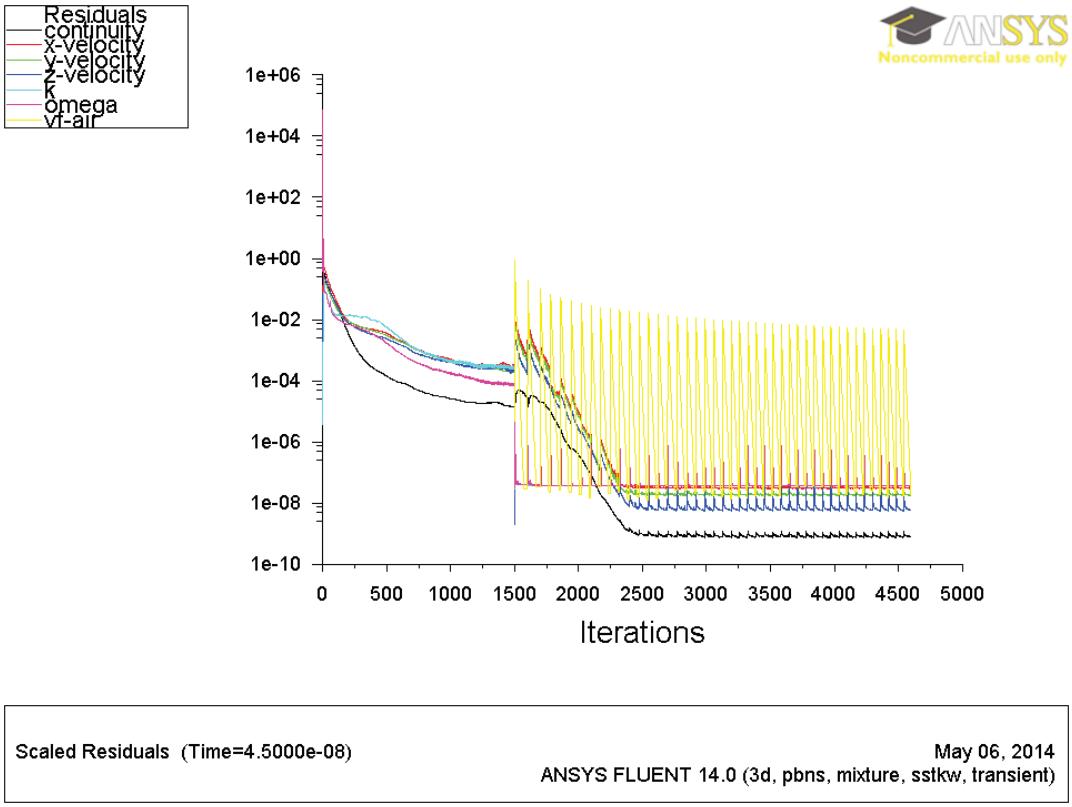

Figure G.2: Part of residual plot for the transient two-phase case

The convergence of each of the time steps are observed. Several residuals are observed and the one which converges last, here the vf-air, is the convergence parameters. Each of the time steps have several iterations. The minimum iteration number per timestep used in the simulations is 15. The iteration number is optimised as the simulation runs.

Appendix H

Forces on the Tube

The simulations are performed without the tube oscillating. In order to see if the oscillations have a significant impact on the simulation results in Section 5.2 a crude analysis of the forces acting on a single bend in the tube will be made. The section of the tube under investigation can be seen in Figure H.1.

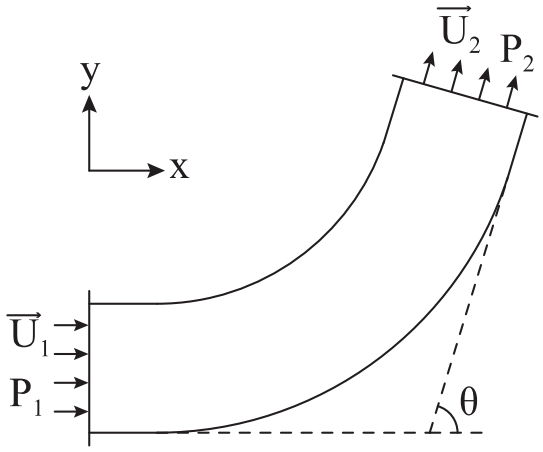

Figure H.1: Free body diagram of the tube bend. Subscript 1 is for the inlet of the bend. 2 is for the outlet bend.

The speed of the fluid and the total pressure forces are area-averaged and extracted using FLUENT. θ is the bending angle of 74°. It is assumed that the inlet and outlet area of the pipe are the same.

H.1 Forces without Oscillations

The fixed control volume under investigation can be seen in H.1. The flow is assumed incompressible. First the total force of the direction change to the fluid will be found in the x- and y-direction which is based on the linear momentum equation [Munson et al., 2010]. Next the pressure change to the fluid in the x- and y-direction will be calculated. In the end the resulting force on the fluid will be given. The calculations will be performed

based on the transient single-phase 350 kg/h liquid flow rate case and the transient two-phase 350 kg/h liquid flow rate with a GVF of 5% case. Subscript 1 is for the inlet of the bend. 2 is for the outlet bend. In the calculation gravity is neglected.

Total force in x-direction:

$$F_{Tx} = \rho\dot{Q}\left(u_{2x} - u_{1x}\right) \tag{H.1}$$
$$u_{1x} = u_1 \tag{H.2}$$
$$u_{2x} = u_2 \cos\left(\theta\right) \tag{H.3}$$

Total force in y-direction:

$$F_{Ty} = \rho\dot{Q}\left(u_{2y} - u_{1y}\right) \tag{H.4}$$
$$u_{1y} = u_1 \sin(0) = 0 \tag{H.5}$$
$$u_{2y} = u_2 \sin\left(\theta\right) \tag{H.6}$$

Pressure forces in x- and y-direction. P_1 and P_2 are total pressures.

$$F_{Px} = P_1 A \cos\left(0\right) - P_2 A \cos\left(\theta\right) \tag{H.7}$$
$$= P_1 A - P_2 A \cos\left(\theta\right) \tag{H.8}$$
$$F_{Py} = P_1 A \sin\left(0\right) - P_2 A \sin\left(\theta\right) \tag{H.9}$$
$$= -P_2 A \sin\left(\theta\right) \tag{H.10}$$

Resulting force:

$$F_{Rx} = F_{Tx} - F_{Px} \tag{H.11}$$
$$F_{Ry} = F_{Ty} - F_{Py} \tag{H.12}$$
$$F_R = \sqrt{F_{Rx}^2 + F_{Ry}^2} \tag{H.13}$$
$$\varphi = \left|\tan^{-1}\left(\frac{F_{Ry}}{F_{Rx}}\right)\right| \tag{H.14}$$

In the calculations the variables listed in Table H.1 are used. The variables are read from the FLUENT simulations.

Variable	Water	Two-phase
Volume flow	$4.8699{\cdot}10^{-5}$	$5.1262{\cdot}10^{-5}$
Fluid density	998.20 kg/m^3	948.37 kg/m^3
θ	74°	74°
u_1	2.19 m/s	2.35 m/s
u_2	2.23 m/s	2.30 m/s
p_1	32660.43 Pa	32784.09 Pa
p_2	32736.49 Pa	32884.97 Pa
A	4.4179e-05 m^2	4.4179e-05 m^2

Table H.1: Variables in the force calculations

The results of the forces in the bend without the oscillations can be found in Table H.2.

Variable	Water	Two-phase
F_{Tx}	-0.0765 N	-0.0805 N
F_{Ty}	0.1042 N	0.1097 N
F_{Px}	1.0443 N	1.0479 N
F_{Py}	-1.3902 N	-1.3965 N
F_{Rx}	-1.1208 N	-1.1284 N
F_{Ry}	1.4944 N	1.5062
F_R	1.8680 N	1.8821
φ	53.13°	53.16°

Table H.2: Results of the force calculations. φ is the angle from the x-axis and up to the force

A sketch of the forces direction and magnitude can be found in Figure H.2.

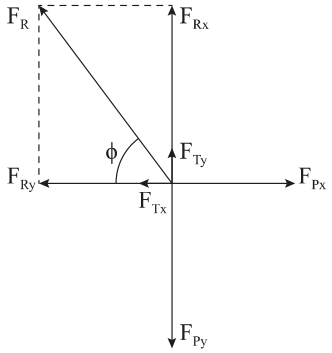

Figure H.2: A sketch of the forces direction and magnitude for the pure water case

H.2 Coriolis Force

The Coriolis force is present due to the oscillations of the tube. It is assumed that the tube only oscillates in the z-direction. The tube oscillates with a different frequency depending on the fluid flowing through the flowmeter. For pure water the frequency is 610.54 Hz and for pure air 700.55 Hz [Basse, 2014b]. Using Equation (H.15) the angular velocity is then 3836.1 rad/s and 4401.7 rad/s in the z-direction, respectively.

$$\vec{\omega} = 2\pi\vec{f} \tag{H.15}$$

For a mixture, following the mixture rules as seen for density, the frequency is 3864.4 rad/s. The oscillation is for the tube swinging back and forth. Examining the forces in one direction, the angular velocity has to be halved.

Equation (H.16) calculates the Coriolis force as seen in Chapter 1.

$$F_c = 2m\frac{\vec{\omega}}{2} \times \vec{U} \tag{H.16}$$

The velocity vector $\vec{U}$ has only a velocity in the x-direction at the inlet of the bend, where the oscillations are given. The value can be seen in Table H.1. Equation H.17 is Equation H.16 for the water case.

$$\begin{aligned} 2m\vec{\omega} \times \vec{U} &= 2m \begin{pmatrix} \omega_y U_z - \omega_z U_y \\ \omega_z U_x - \omega_x U_z \\ \omega_x U_y - \omega_y U_x \end{pmatrix} \\ &\overset{\text{for water}}{\rightarrow} \approx 2 \cdot 0.0018\text{kg} \begin{pmatrix} 0 \\ \frac{3836.1\text{rad/s}}{2} \cdot 2.19\text{m/s} \\ 0 \end{pmatrix} = 15.4\text{N} \end{aligned} \tag{H.17}$$

A rough estimation of the 1/4 of the mass in the tube is 0.0018 kg for pure water and 0.0017 kg with a GVF of 5%. The mass estimations are based on a straight pipe with the tubes length (166 mm) and diameter (7.5 mm).

The size of the Coriolis force does not change significantly when introducing 5% air to the liquid flow. Using Equation H.16 the following estimations for the Coriolis force for the pure water and the mixture with a GVF of 5% case.

$F_{c,\text{ single-phase - water}} \approx 15.4$ N in y-direction
$F_{c,\text{ two-phase}} \approx 15.5$ N in y-direction

A simple sensitivity analysis of the calculations performed in Section H.2 shows that a doubling of the mass in the bend will double the Coriolis force. Since the mass is estimated based on a straight pipe, the mass estimation is lower than in the actual curved bend. So the rough estimation of the Coriolis force shall be seen as a minimum value due to the uncertainty of the mass estimations.

The resulting forces acting on the fluid, whether it is single- or two-phase, are very similar. The Coriolis force is approximately 15.5 N in the y-direction. The Coriolis force is approximately 8 times larger than the resulting force acting on the fluid.